Estimating northern hemisphere snow water equivalent for climate research through assimilation of space-borne radiometer data and ground-based measurements

Matias Takala [a,*], Kari Luojus [a], Jouni Pulliainen [a], Chris Derksen [b], Juha Lemmetyinen [a], Juha-Petri Kärnä [c], Jarkko Koskinen [a], Bojan Bojkov [d]

[a] Finnish Meteorological Institute, Finland
[b] Environment Canada, Canada
[c] Finnish Environment Institute, Finland
[d] European Space Agency, Italy

ABSTRACT

The key variable describing global seasonal snow cover is snow water equivalent (SWE). However, reliable information on the hemispheric scale variability of SWE is lacking because traditional methods such as interpolation of ground-based measurements and stand-alone algorithms applied to space-borne observations are highly uncertain with respect to the spatial distribution of snow mass and its evolution. In this paper, an algorithm assimilating synoptic weather station data on snow depth with satellite passive microwave radiometer data is applied to produce a 30-year-long time-series of seasonal SWE for the northern hemisphere. This data set is validated using independent SWE reference data from Russia, the former Soviet Union, Finland and Canada. The validation of SWE time-series indicates overall strong retrieval performance with root mean square errors below 40 mm for cases when SWE <150 mm. Retrieval uncertainty increases when SWE is above this threshold. The SWE estimates are also compared with results obtained by a typical stand-alone satellite passive microwave algorithm. This comparison demonstrates the benefits of the newly developed assimilation approach. Additionally, the trends and inter-annual variability of northern hemisphere snow mass during the era of satellite passive microwave measurements are shown.

© 2011 Elsevier Inc. All rights reserved.

1. Introduction

The seasonal snow cover of the northern hemisphere has a major effect on climate, the water cycle, and biogeochemical cycling. The winter season surface albedo in northern land areas is controlled by snow extent, as the difference in the reflectance of snow and snow-free ground is high. Terrestrial run-off is dominated by snow and glacier mel at mid- and high latitudes and high elevation areas across Eurasia and North America regions (Barnett et al., 2005). The carbon balance at northern latitudes is influenced by the length of the snow season, particularly the timing of snow melt. The respiration of soil, as well as the thickness of the seasonally thawing active layer in permafrost areas is related to the timing of snow melt as well as the seasonal evolution of snow mass (Grogan and Jonasson, 2006). Improved information on snow cover, therefore, provides a tool to further investigate climatological, hydrological, and greenhouse gas processes (such as CO2 and CH4) at middle and high latitudes.

Snow water equivalent (SWE) is the product of snow depth (SD) and snow density (ρ) and represents the resulting water column should a snowpack melt in place. For the purposes of climate research, SWE or SD can be estimated using the interpolation of ground-based observations (for example, Dyer and Mote, 2006; Kitaev et al., 2002) although these interpolation methods can lack temporal resolution and are negatively impacted by the sparse spatial coverage of observations particularly in northern regions. Improvements to interpolation techniques by applying various kriging approaches have been suggested e.g. by Hudson and Wackernagel (1994), Erxleben et al. (2002) and Brown and Tapsoba, (2007). Information on snow cover extent (SE) and SWE/SD can be also obtained from atmospheric reanalysis datasets (for example, as described in Brown et al., 2010) or by assimilating data from different sources. For example, the Canadian Meteorological Centre (CMC) produces a daily gridded global snow depth analysis by combining all available snow observations with a simple snow model (Brasnett, 1999) while the National Weather Service produces daily snow information for the continental United States and parts of southern Canada through a snow analysis system that also combines observations with a snow model (Carroll et al., 2006; Rutter et al., 2008). The point-wise nature of in situ measurements, however, remains in these products. For instance, the CMC analysis has a tendency

* Corresponding author at: Finnish Meteorological Institute, P.O. BOX 503 FI-00101 Helsinki, Finland. Tel.: +358 40 5279 778.
E-mail address: matias.takala@fmi.fi (M. Takala).

towards early loss of snow cover in the spring due to the shallow bias of snow depths reported from observing sites that tend to be located in clearings (Brown et al., 2010).

For climate applications, long time series are needed in order to produce meaningful statistics on trends and variability. Satellite passive microwave data are commonly used for the retrieval of snow information because of a wide swath (which produces frequent repeat coverage), insensitivity to illumination and decreased influence of clouds, multi-frequency response to the presence of snow on land, and of the availability of a continuous time series that extends back to 1978 (Table 1). The limiting factor for the climatological use of passive microwave derived SWE information is the high uncertainty in SWE and SD retrievals at the hemispheric scale both in terms of systematic and random error (i.e. Kelly et al., 2003). Most passive microwave SWE retrieval algorithms exploit the negative spectral gradient between a measurement frequency sensitive to snow grain volume scattering (~37 GHz) and a measurement frequency considered largely insensitive to snow (~19 GHz; Chang et al., 1987, 1990; Goodison and Walker, 1995; Kelly et al., 2003; Mognard and Josberger, 2002; Pulliainen, 2006). The larger the difference between brightness temperature (T_B) measurements at these two frequencies, the higher the estimate of SWE.

The algorithm originally proposed by Chang et al. (1987) estimated snow depth from horizontally polarized Scanning Multichannel Microwave Radiometer (SMMR) measurements. The algorithm has a physical basis — the parameterization was based on forward simulations with a radiative transfer model. This algorithm has been widely adopted for estimating SWE from different space-borne microwave radiometers (Armstrong and Brodzik, 2001) including modifications to account for variable surface and snowpack characteristics (Foster et al., 1997, 1991; Tait, 1998). Armstrong and Brodzik (2002) compared the performance of several traditional algorithms (Chang et al., 1987, Goodison, 1989; Nagler and Rott, 1992; Rott et al., 1991) and found large errors at the hemispheric scale when compared to available in situ data. The general tendency was for the algorithms to underestimate SWE, especially under deep snow conditions, while algorithm performance broke down completely under wet snow conditions. Large errors (approaching 100%) were reported in the hemispheric application of T_B difference algorithms by Kelly et al. (2003) with lake-rich tundra areas proving especially problematic for this approach (Derksen et al., 2010; Koenig and Forster, 2004). When applied regionally, land cover specific T_B difference algorithms have reported lower uncertainties (Derksen, 2008; Derksen et al., 2010, 2005), although consistent underestimation of SWE occurs in heavily forested areas and the accuracy characteristics are subject to inter-seasonal variability due to changes in snowpack physical properties (e.g. when ice lenses are present).

A different approach is the use of theoretical or semi-empirical radiative transfer models for snow cover, coupled with atmospheric and vegetation models, to simulate microwave emission and inversely calculate snow characteristics from satellite measurements (e.g. Pulliainen et al., 1999, Wiesmann and Matzler, 1999). The more complicated models are computationally expensive and require precise ancillary data in order to give accurate predictions (i.e. Durand and Margulis, 2006). These factors restrict their operational applicability on a global scale.

Improving the performance of passive microwave retrieval algorithms by means of data assimilation has also been investigated. Pulliainen (2006) presents an assimilation technique which weighs passive microwave data combined with a semi-empirical radiative transfer model, and prior snow information from ground measurements, with their respective statistical uncertainties. This technique successfully reduced systematic errors related to the saturation of T_B difference algorithms when SWE exceeds approximately 120 mm. In regional studies by Pulliainen and Hallikainen (2001) and Pulliainen (2006) unbiased RMSE values of 15 to 40 mm were achieved when compared to in situ data.

In this study, we implement the methodology of Pulliainen (2006) across the northern hemisphere to exploit the benefits of both conventional measurements and passive microwave data to produce a Climate Data Record (CDR) for SWE. The approach of Pulliainen (2006) is enhanced by integrating the methodologies of Hall et al. (2002) and Takala et al. (2009) to discriminate the region of dry seasonal snow cover and estimate the date the land surface becomes snow free. As it is based on the assimilation of ground-based synoptic observations of SD and space-borne radiometer data, benefits of the approach are that SWE (and SD) estimates are produced for wet snow cover, and statistical error variance estimates are provided for every individual SWE estimate (produced on a grid with a resolution of 25 km).

Because this study is concerned with the production of snow cover information for climate trend analyses and for the evaluation of climate models, an essential aspect is the validation of the 30 year SWE time series. Typically, snow course observations representative for coarse grid cell evaluation are lacking at a continental scale over long time periods. In this study, however, we utilize the Russian INTAS-SCCONE (International Association for the promotion of co-operation with scientists from the New Independent States of the former Soviet Union — Snow Cover Changes Over Northern Eurasia) snow surveys as independent reference data for validation. These data are available throughout the former Soviet Union between 1980 and 2000, with observations from a total of 1292 snow courses. The Russian sites are complemented by Finnish snow surveys including SWE observations from years 2005–2008, and Canadian research data sets on SWE for tundra, boreal forest, and prairie environments also for 2005–2008.

The specific objectives of this study are to:

1. provide an overview of the SWE retrieval technique (based on Pulliainen, 2006) now applied across the northern Hemisphere within the European Space Agency (ESA) GlobSnow project (Luojus et al. 2010).
2. assess these SWE retrievals against reference SWE measurements and compare the retrieval accuracy to other available algorithms.
3. develop a climatological time series (1979 to 2010) of northern hemisphere SWE (and total/continental snow mass).

2. Methods and data

2.1. Algorithm overview

The methodology for SWE retrieval employed in this study utilizes a Bayesian non-linear iterative assimilation approach first described

Table 1
Summary of satellite passive microwave sensors.

Platform	Sensor	Frequency (GHz)	Swatch width (km)	Incidence angle (degrees)	Field of view (km)
Nimbus-7 (1987)	SMMR	6.6	800	50.3	95×148
		10.69			70×109
		18.0			43×68
		21.0			36×56
		37.0			18×27
DMSP F8 to F-15 (1987)	SSM/I	19.4	1400	53	45×70
		22.2			40×60
		37.0			30×38
		85.5			14×16
Aqua (2002)	AMSR-E	6.9	1445	54.8	43×75
		10.7			29×51
		18.7			16×27
		23.8			18×32
		36.5			8×14
		89.0			4×6

in Pulliainen (2006). A flowchart of the algorithm is presented in Fig. 1; there are four primary steps to the retrieval scheme:

Step 1 Snow Depth (SD) observations from synoptic weather stations are obtained for the northern hemisphere from the European Centre for Medium-Range Weather Forecasts (ECMWF; this dataset is described further below). The uncertainty of synoptic SD observations is estimated by assigning a variance of 150 cm^2 (a value based on a comparison of point-wise synoptic SD data with available coincident snow survey data sets). The stations located in mountainous areas are filtered out, as are the deepest 1.5% of reported snow depth values in order to avoid spurious or erroneous deep snow observations. The mountain mask criterion is to remove all observations that fall within Equal Area Scaleable Earth Grid (EASE-Grid) cells with a height standard deviation above 200 m within the grid cell. Once this filtering is performed, an 'observed SD' field is produced from the synoptic weather station observations by ordinary kriging interpolation to the 25 km EASE-Grid. An estimate of the interpolation variance is also obtained. The exponential autocorrelation function of the spatial variability of snow depth is calculated for each day by separately analyzing the observations for North America and Eurasia.

Step 2 The available synoptic weather station measurements of snow depth are used as input to forward model simulations of brightness temperature (T_B) using the single layer HUT snow emission model (Pulliainen et al., 1999). The applied version of the model describes the scene brightness temperature as a

function of the characteristics of a single-layer snow pack (depth, bulk density and grain size) and forest canopy (stem volume/biomass). Additionally, the approach takes into account atmospheric effects on space-borne T_B measurements. The model is fit to satellite observed T_B values at the locations of weather stations by optimizing the value of effective snow grain size. The satellite radiometer measurements are taken from the sensors summarized in Table 1, depending on the year. The fitting procedure is:

$$\min_{d_0} \left\{ \left(T_{B,19V,\text{mod}}\left(d_0, D_{ref}\right) - T_{B,37V,\text{mod}}\left(d_0, D_{ref}\right) \right) \right. \tag{1}$$

$$\left. - \left(T_{B,19V,obs} - T_{B,37V,obs} \right) \right\}^2$$

where the known snow depth is D_{ref}, $T_{B,19V}$ and $T_{B,37V}$ denote the vertically polarized brightness temperature at approximately 19 and 37 GHz with sub-indices *mod* and *obs* referring to modeled and observed values, respectively. Vertical polarization is used because it correlates best with SWE in the boreal forest zone (Hallikainen and Jolma 1992, Pulliainen et al., 1999, Pulliainen and Hallikainen 2001) The HUT model describes T_B as a function of SWE, snow density and snow grain size, d_0 in Eq. (1). Here, snow density is treated with a constant value of 0.24 g/cm^3, a reasonable 'global' value given by the analysis of Sturm et al., 2010. The observed snow depth at a weather station is used as input to Eq. (1). At each
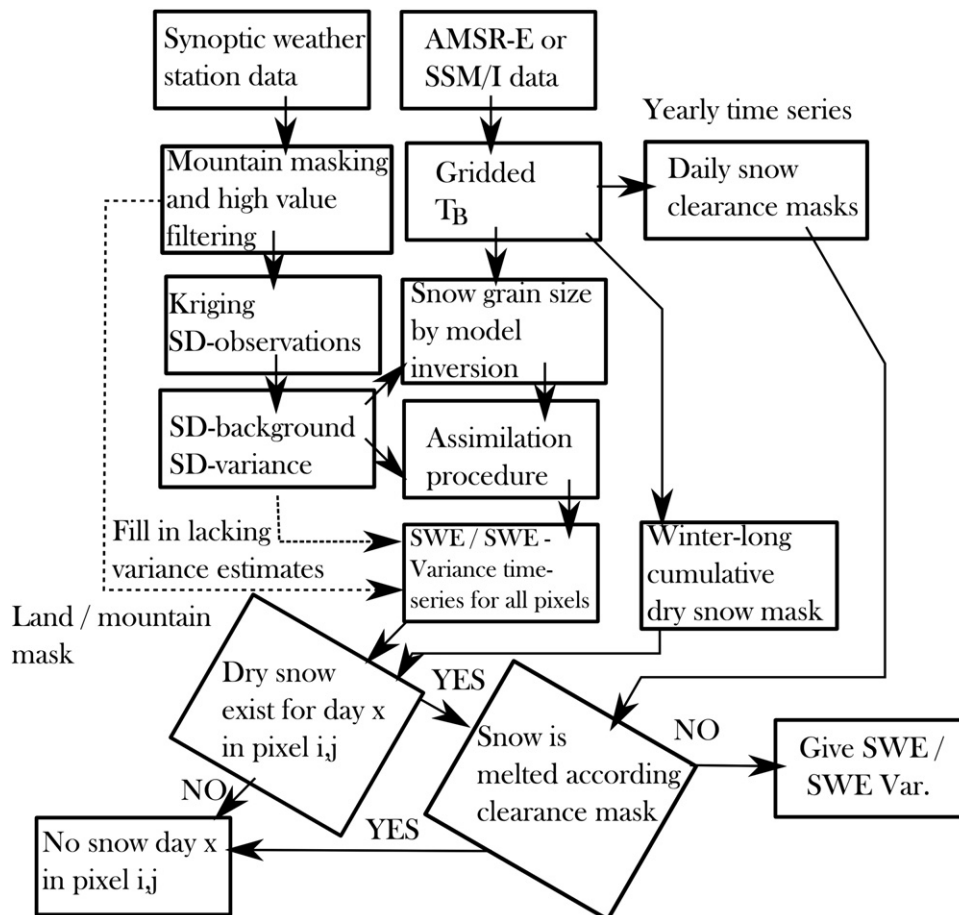

Fig. 1. Processing chain for SWE retrievals.

synoptic station location, the final estimate of the grain size (and its standard deviation λ) is obtained by averaging values obtained for the ensemble of the nearest stations:

$$\left\langle \hat{d}_{0,ref} \right\rangle = \frac{1}{M} \sum_{j=1}^{M} \hat{d}_{0,ref,j} \tag{2.a}$$

$$\lambda_{d0,ref} = \sqrt{\frac{1}{M-1} \sum_{j=1}^{M} \left(\hat{d}_{0,ref,j} - \left\langle \hat{d}_{0,ref} \right\rangle \right)^2} \tag{2.b}$$

where M is the number of stations (neighborhood of 6 stations used in this paper). The lower bound for the grain size is set to 0.2 mm with smaller values rounded up.

Step 3 A spatially continuous background field of the effective snow grain size (including a variance field) is interpolated using a kriging technique from the snow grain size estimates produced for the weather station locations in Step 2.

Step 4 A map of spatially continuous 'assimilated SWE' is produced through forward Tb simulations with the HUT model using the interpolated effective grain size produced through Steps 2 and 3 and land cover information (dataset described below). The simulations are compared with spaceborne radiometer measurements via a cost function at each grid cell with spaceborne radiometer measurements. The cost function also considers the "*observed SD*" background field. Model estimates are matched to observations numerically by fluctuating the SWE value. The cost function constrains the grain size value according to the predicted background grain size and the estimated variance produced in Step 3. Thus, the assimilation adaptively weighs the space-borne brightness temperature observations and the '*observed SD*' field (produced in Step 1) to estimate a final SWE and a measure of statistical uncertainty (in the form of a variance estimate) on a grid cell by grid cell basis:

$$\min_{D_t} \left\{ \left(\frac{\left(T_{B,19V,\text{mod}}(D_t) - T_{B,37V,\text{mod}}(D_t) \right) - \left(T_{B,19V,obs} - T_{B,37V,obs} \right)}{\sigma_t} \right)^2 \right.$$
$$\left. + \left(\frac{D_t - \hat{D}_{ref,t}}{\lambda_{D,ref,t}} \right)^2 \right\} \tag{3}$$

where $\hat{D}_{ref,t}$ is the snow depth estimate from the kriging interpolation for the day under consideration, t in Eq. (3). $\lambda_{D,ref}$ the estimate of standard deviation from the kriging interpolation, and D_t is the snow depth for which Eq. (3) is minimized (note that $D_t = SWE/(0.24\ g/cm^3)$). The variance of the T_B is σ_t. It can be estimated by approximating T_B (a function of snow depth and grain size) by a Taylor series:

$$T_B(D_t, d_0) \approx T_B\left(D_t, \left\langle \hat{d}_{0,ref,t} \right\rangle \right) + \frac{\partial T_B\left(D_t, \left\langle \hat{d}_{0,ref,t} \right\rangle \right)}{\partial d_0} \left(d_0 - \left\langle \hat{d}_{0,ref,t} \right\rangle \right) \tag{4.a}$$

$$\sigma_t^2 = \text{var}\left(T_B\left(D_t, \left\langle \hat{d}_{0,ref,t} \right\rangle \right) \right) = \left(\frac{\partial T_B\left(D_t, \left\langle \hat{d}_{0,ref,t} \right\rangle \right)}{\partial d_0} \right)^2 \lambda_{d0,ref,t}^2 \tag{4.b}$$

The variance σ_t^2 in Eqs. (3) and (4.b) is a parameter that adjusts the weight of brightness temperature data with respect to the weight of the '*observed SD*' field (parameter $\lambda_{D,ref}$). A basic feature of the algorithm is that if the sensitivity of space-borne radiometer observations to SWE is assessed to be close to zero by formulas (4.a) and

(4.b), the weight of the radiometer measurements on producing the '*assimilated SWE*' approaches zero (this is the case e.g. if the magnitude of SWE is very high). The higher the estimated sensitivity of T_B to SWE, the higher the weight given to the radiometer data. Thus, the weight of the radiometer data varies both temporally and spatially in order to provide a maximum likelihood estimate of SWE.

A comparison of point-wise ECMWF SD-observations with really distributed snow surveys (INTAS-SCONE data set covering Russian and Finnish snow courses, see Section 2.2 below) indicated a random difference with a variance level of about 100–150 cm². Thus, a variance of 150 cm² was attributed to SD measurements at the location of weather stations (this is also considered by $\lambda_{D,ref}$ in Eq. (3)). While it is possible to use previous SWE estimates in the assimilation algorithm (Pulliainen, 2006), in this work the SWE is estimated on a per day basis with no consideration of previous retrievals.

In order to provide a hemispheric SWE map for the region of seasonal snow cover, it is also necessary to produce a cumulative dry snow mask for each snow cover season (beginning September 1). For this purpose, the dry snow detection algorithm of Hall et al. (2002) is applied to satellite radiometer data. From satellite passive microwave measurements, the date of snow clearance can also be estimated using the algorithm of Takala et al. (2009). If the cumulative dry snow mask shows that a grid cell in question for a particular date has never been marked as dry snow it is labeled as snow free through the winter. If the cumulative dry snow mask suggests that the pixel has had dry snow conditions, but is already snow free according to the snow clearance algorithm, the pixel is marked as snow free. An estimate of the SWE and SWE variance is given for grid cells for which dry snow cover has been detected and for which snow melt has not yet been indicated (note that for wet snow cover the algorithm inherently assesses the weight of radiometer data to approach zero). If a grid cell is in a mountainous area it is flagged as such and no SWE is retrieved due to the uncertainty of microwave measurements in complex, snow covered Alpine terrain (for example, Tong et al., 2010).

2.2. Input data for dataset development

2.2.1. ECMWF snow depth data

Daily SD background fields were generated from observations at synoptic weather stations acquired from ECMWF for the years 1978–2010 (supplemented by INTAS SCCONE data described below). For each measurement, a WMO station identifier, date of measurement, and snow depth (SD) are given. There are no error estimates for the snow depth measurements provided with the ECMWF dataset. The snow depth is traditionally manually measured with a rod or ruler, although in the 1990s there was a transition to automated snow depth sensors in many countries. As noted in Section 2.1, we account for uncertainty in the point snow depth measurements by assigning a variance of 150 cm² to the observations (based on comparison of point-wise data with coincident snow course measurements from Finland). An unpublished evaluation of point versus transect snow survey measurements from the Environment Canada archive produced a similar variance value.

2.2.2. INTAS SCCONE snow depth data

The ECMWF SD data were enhanced with the inclusion of the INTAS-SCCONE snow depth dataset (Kitaev et al., 2002). This improves the density of surface observations across the former Soviet Union. Manual SD measurements are available for 223 different locations. In addition to information on WMO station identifier, date of measurement and SD, a qualitative estimate of the snow covered area and a status flag value are given. The flag describes whether the observed snow melt was temporary or continuous, and whether the value of SD is correct or should be rejected. The dataset also contains a short description of station characteristics, for example information on whether the station is protected from strong winds or not.

2.2.3. Satellite radiometer data

A complete time series of radiometer data from 1978 to 2010 was acquired from the National Snow and Ice Data Center (NSIDC) in Boulder, Colorado USA. For the years 1978–1987, the Scanning Multi-channel Microwave Radiometer (SMMR; Knowles et al., 2002) data from Nimbus 7 were used, whereas for 1987–2010, the Special Sensor Microwave/Imager (SSM/I; Armstrong et al., 1994) data from Defense Meteorological Satellite Program (DMSP) D-11 and D-13 are used. For the years 2002–2010 data from Advanced Microwave Scanning Radiometer (AMSR-E; Knowles et al., 2006) onboard the Aqua satellite were acquired. We made no adjustments for any possible inter-sensor bias in the satellite time series. The unadjusted data sets from different passive microwave sensors are not directly comparable in absolute levels, but may include some biases from one instrument to another, however, a benefit of the SWE mapping methodology applied here is that it reduces the effects of these biases.

The space-borne T_B measurements are in the EASE-Grid north azimuthal equal-area projection with a nominal resolution of 25 km × 25 km (Armstrong et al., 1994). The local overpass time varies but the difference between randomly chosen dates is not larger than 2 h. The descending orbit measurements correspond to the early morning (0500 to 0700 local time) and ascending orbit measurements correspond late afternoon (1500–1700 local time), although in the case of SSM/I the local overpass time (ascending vs. descending) depends on which DSMP satellite the instrument was onboard. Data used in this paper are a combination of ascending and descending orbits, utilized in such a way that day-time passes are applied only to the areas where no nighttime passes are available. This enhances the spatial coverage without deteriorating the overall accuracy.

The most important frequencies for snow detection and SWE retrieval are 19 and 37 GHz. As shown in Table 1, channels close to these frequencies are available from all instruments, although with different native footprint dimensions. These differences in swath level resolution are removed through T_B re-sampling to the EASE-Grid as described in Armstrong et al. (1994). Some data gaps exist both in time and space within the satellite passive microwave data record. SMMR had a narrow swath width (600 km) and was de-activated every other day due to power constraints.

2.2.3. Land use and topographic data

The Global Land Cover 2000 was used as land use information for the assimilation algorithm (http://bioval.jrc.ec.europa.eu/products/glc2000/glc2000.php). The dataset covers the whole globe at a resolution of 1 km with 23 land cover classes. Areal fractions of two basic land cover categories were calculated for each EASE-Grid cell and inputted to the forward T_b model in the assimilation scheme. The two applied land cover classes were (a) forest and (b) all other land cover classes. Grid cells with major lakes were masked out if the areal fraction of open water exceeded 50%. The approximate forest biomass (stem volume) was assigned to the forest fraction of each grid cell. For North America, a mean forest stem volume value of 80 m³/ha was used to characterize the effect of forest cover based on FAO statistics (http://www.fao.org/forestry/32042/en/). While this is a very generalized approach, estimation of effective grain size
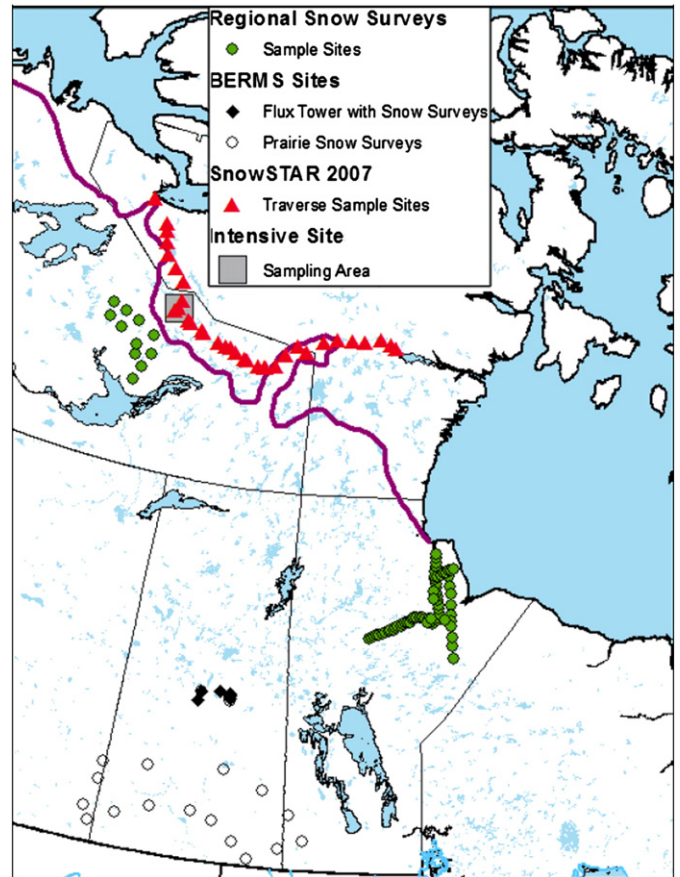

Fig. 3. Overview of reference datasets for Canada.

greatly reduces the sensitivity of the algorithm to forest biomass allowing a constant value to be adopted. For northern Eurasia, a spatially varying stem volume value was assigned to the forest fraction of each grid cell based on a digital forest map described in Bartalev et al. (2004).

Topographic information for the masking of complex terrain was derived from ETOPO5 (National Geophysical Data, 1988) data. This dataset contains global elevation information at a resolution of 5 arc minutes, an appropriate resolution given the scale of the 25 km EASE-Grid.

3. Reference measurements for dataset evaluation

3.1. INTAS-SCCONE snow course data

The INTAS-SCCONE data set includes snow course observations from an extensive network across the former Soviet Union and Russia (Kitaev et al., 2002). These data are independent from the INTAS-SCCONE point snow depth data used as part of the SWE algorithm input. The snow surveys occurred bi-monthly at 1264 sites (total of 424,600 samples), and extend from 1978 to 2000 (Fig. 2). The snow
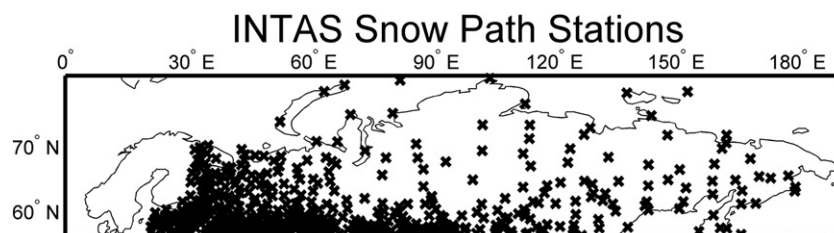

Fig. 2. Location of INTAS-SCCONE reference snow paths.

course data were collected using three procedures depending on the landscape (Karpechko, personal communication). In closed forests the length of the snow survey was 500 m with snow depth measured at 10 m intervals, and snow density every 100 m. In open canopy forested regions the length of the snow survey was 1000 m, while in steppes the length of snow survey was 2000 m. For both of these land cover types, snow depth was measured every 20 m, and snow density sampling was conducted at 200 m intervals (although measurements were sometimes made every 100 m). Measured snow depth and snow density were averaged along the path, and water equivalent calculated as $SWE = 10dh$ (mm), where d = density (g/cm3) and h = depth (cm).

3.2. Snow course data from Finland

Finland has a comprehensive network of 165 snow survey sites operated by the Finnish Environment Institute (SYKE) (Kuusisto 1984; Perala and Reuna, 1990). The measurements are made once or twice in a month, and include both SWE and fractional snow coverage (FSC). Each snow course is 2 to 4 km long, and covers the various terrain types found around each site. The measurement procedure is similar to that of INTAS-SCCONE snow surveys, so these measurements are similarly well suited for validating coarse resolution SWE retrievals.

3.3. Canadian reference datasets

In order to evaluate coarse resolution satellite retrievals and climate model simulations, Environment Canada has augmented the sparse Canadian national snow survey network with field measurement campaigns designed to provide regionally representative snow measurements (see Fig. 3). Measurements of snow physical properties were made at a network of sites across northern Manitoba during late winter 2004 through 2007, and the Northwest Territories from 2005 to 2008 Snow cores were taken for direct measurement of SWE and bulk density, snow depth measurements were made to characterize local-scale variability, and snow pits were excavated for snowpack stratigraphy measurements including density profiles and grain size. These measurements are described further in Derksen (2008).

Intensive tundra snow surveys (snow water equivalent, depth, density, and stratigraphy) were performed in the Daring–Exeter–Yamba watershed of the Upper Coppermine River Basin in the Northwest Territories Canada near the timing of peak SWE, April 2004 through 2010. A stratified sampling approach was utilized to determine slope, aspect, and land cover controls on snow properties. During April 2007, a coordinated series of snow measurements were made across the Northwest Territories and Nunavut, Canada during a snowmobile traverse from Fairbanks, Alaska to Baker Lake, Nunavut.
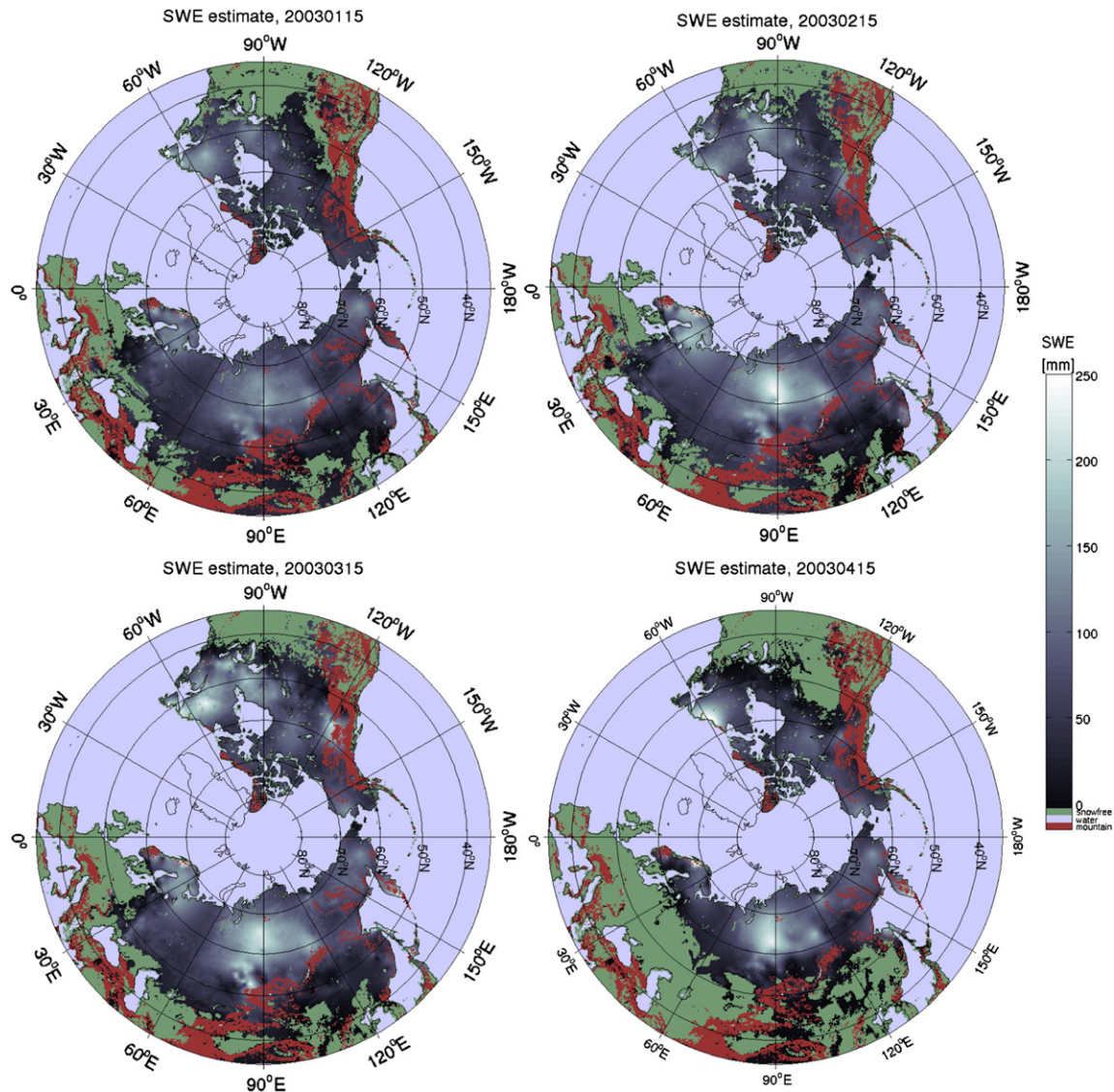

Fig. 4. Example SWE maps from the winter of 2003. The snow line indicates the line of snow clearance as determined from the satellite T_b data.

Sample sites were located at least every 1° of longitude. At these sites, snow depth, density, SWE, stratigraphy, and grain size were measured (see Derksen et al., 2009).

The Boreal Ecosystem Research and Monitoring Sites (BERMS) program was a joint initiative of Canadian government agencies, universities and other research partners. The main objective was to study the role that the Canadian boreal forest plays in the global carbon budget in response to climate change. Snow depth was measured at 30 minute intervals with SR-50 sonic snow depth gages at sites representative of old growth boreal forest (aspen, black spruce, jack pine), a chrono-sequence of harvested sites (1975, 1994, 2002), fire disturbed stands (1977, 1989, 1998), and a boreal fen.

Bi-weekly snow course measurements (direct measurements of depth, density and SWE) are also available both at the BERMS sites, and similar forest cover types in the same region. Bi-weekly snow surveys at open prairie sites south of the boreal forest are also available from Environment Canada. These prairie measurements take into account different agricultural land use (i.e. fallow vs. stubble fields) through multiple sampling transects.

4. Results

4.1. Overview of results

Daily SWE estimates were produced for the years 1979–2009 using the retrieval procedure described in Section 2. Input satellite measurements were from SMMR (1979–1987), SSM/I (1987–2002) and AMSR-E (2002–2009). The daily estimates were averaged with a sliding 7-day window in order to reduce the noise level in the daily time series. The sliding average corresponds, in practice, to the output of the filtering approach described in Pulliainen (2006). Fig. 4 depicts an example of the hemispheric output of the algorithm for four dates in the winter of 2003. The estimate for the total snow covered region is conservative for early winter due to the dry snow detection algorithm (Hall et al., 2002). In mid-winter and during spring the snow line and its retreat north is better captured, as illustrated earlier for Eurasia using the same snow melt algorithm (Takala et al., 2009).

Fig. 5 illustrates the difference between the final assimilation result and the ground data based interpolation. This represents the difference between the '*observed SD*' field (multiplied with a constant snow density of 0.24 g/cm³) and the '*assimilated SWE*' field as described in Section 2. This demonstrates the impact of incorporating satellite passive microwave data compared to the use of ground data interpolation only. Fig. 5a shows an example of a single hemispheric difference map, whereas Fig. 5b depicts the histogram of the difference for the 30-year-long daily time series. The maximum values of the difference in SWE extend to about 100 mm. However, the number of such cases is small, and therefore not evident in Fig. 5b. As indicated by Fig. 5a the spatial variability of the weight of the satellite input varies strongly depending on the coverage of weather stations used as input to the assimilation algorithm. The weight also varies temporally, being low if the sensitivity of SWE to observed brightness temperature is estimated to be low. Previous investigation (Pulliainen, 2006) shows that the assimilation approach improved the SWE estimation accuracy in about 60% of the investigated cases across Eurasia (the improvement was also typically larger than any reductions) compared with the interpolation of weather station SD values only.

4.2. Algorithm assessment

The SWE estimates were evaluated using independent reference datasets for three regions: Finland, Eurasia, and Canada. The SWE estimates were taken from daily hemispheric output of the retrieval scheme averaged with a sliding 7-day window (For instance, the
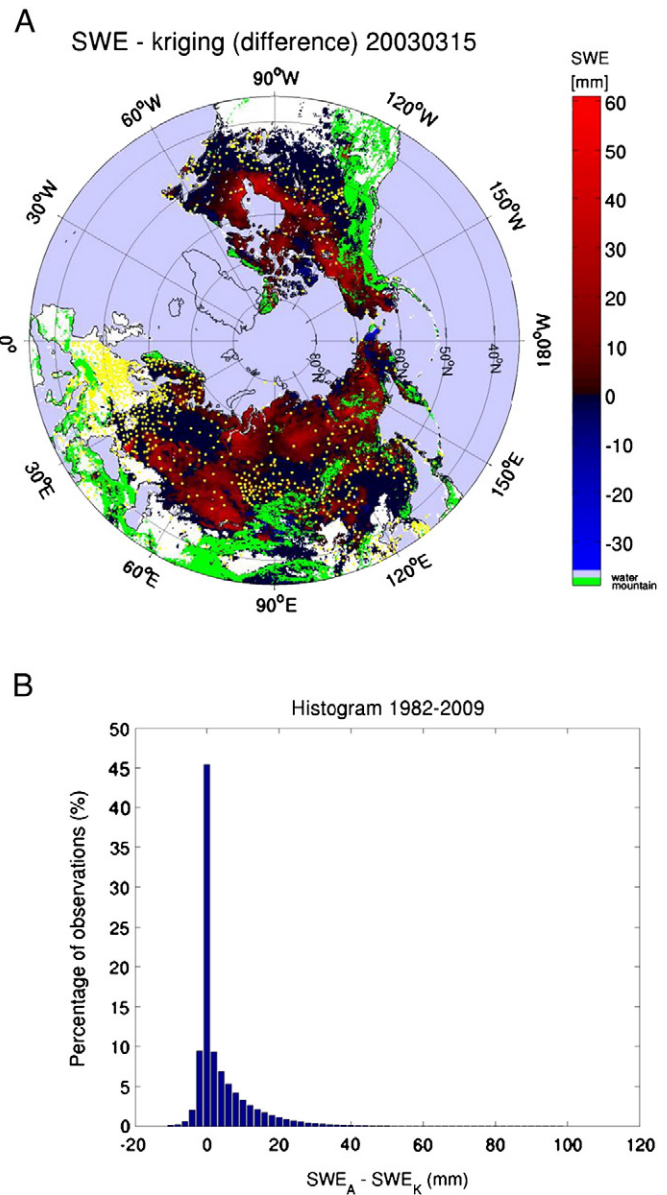
Fig. 5. Difference between assimilated SWE and background field of SWE interpolated from synoptic weather station data. (a) Example of difference map for 15 March, 1993 (single day estimate). The locations of snow depth reporting weather stations are also indicated by yellow dots. Mountains are masked by green color. (b) Histogram of the difference for the complete data set from 1979 to 2010 (as determined from 7-day sliding average estimates).

SWE estimate for 7 January is an average of the assimilation scheme output for 1 to 7 January). Thus, a consistent implementation of the algorithm was evaluated for all three test regions.

4.2.1. Finland

Fig. 6 shows the relationship between SWE estimates and measured values from snow courses in Finland for November through May, covering 2005 to 2008. The assimilation algorithm performs very well when SWE is less than approximately 150 mm, with systematic SWE underestimation evident above this threshold. The exact value of this limit varies according to snow grain size and the stratification of snow pack, as illustrated in many previous studies (De Sève et al., 1997, 2007; Lemmetyinen et al., 2010; Mätzler, 1994; Rosenfeld and Grody, 2000). The highest SWE values are consistently found in the same geographic region in northern Finland.
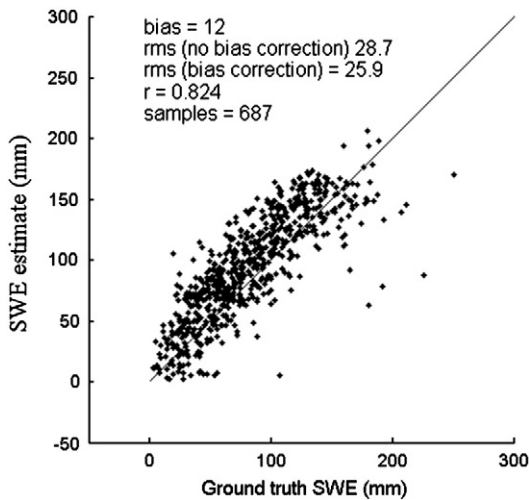
Fig. 6. SWE algorithm performance over Finland versus national snow course observations.

Passive microwave SWE retrieval algorithms have a well documented tendency to systematically underestimate SWE under deep snow conditions due to a change in the microwave behavior of the snow-pack (when SWE exceeds approximately 150 mm, the snowpack transitions from a scattering medium to a source of emission). The increasing proportion of areas with high SWE values as winter progresses increased the overall errors during the late winter and spring, however the RMS errors remained below 40 mm for all months except April 2007. In addition to SWE underestimation under deep snow conditions driven by decreased sensitivity of the radiometer measurements, the fixed snow density of 0.24 g/cm^3 tends to decrease SWE estimates for late winter when snowpacks, which are often denser. The overall strong performance of the assimilation algorithm was expected for this region because of the dense network of weather station inputs available across Finland (approximately 40 WMO synoptic stations in the region of 330 000 km^2).

4.2.2. Eurasia

A comparison of SWE estimates produced from the assimilation algorithm with INTAS-SCCONE snow course observations is shown in Figs. 7 and 8. The assessment was performed from 1980 to 2000. A summary of seasonal performance statistics is provided in Table 2 considering the full range of SWE reference observations. The seasonal performance was assessed separately for fall, winter and spring; September–December, September–March and April–May, respectively. Again, sensitivity to increasing SWE decreases when SWE values exceed the level of about 150 mm.

SWE retrievals were also compared with the snow course measurements in order to determine the interannual variability in the uncertainty (considering whole winter period). As shown in Fig. 8, the RMS error and bias fluctuate from season to season, but across a relatively narrow range (RMSE of about 30 to 40 mm; and a bias ranging from −3 to +9 mm when SWE <150 mm indicating that a small bias is possible). When all snow course measurements are considered the RMS error increases to 45 mm and a bias of −5 mm is observed. This again indicates a tendency of SWE underestimation for deep snow packs.

4.2.3. Canada

An overall assessment of algorithm performance was achieved by comparing SWE retrievals with reference ground measurements for various Canadian land cover regions. The overall RMS and coefficient of determination (R^2) values for the Canadian data were 40 mm and
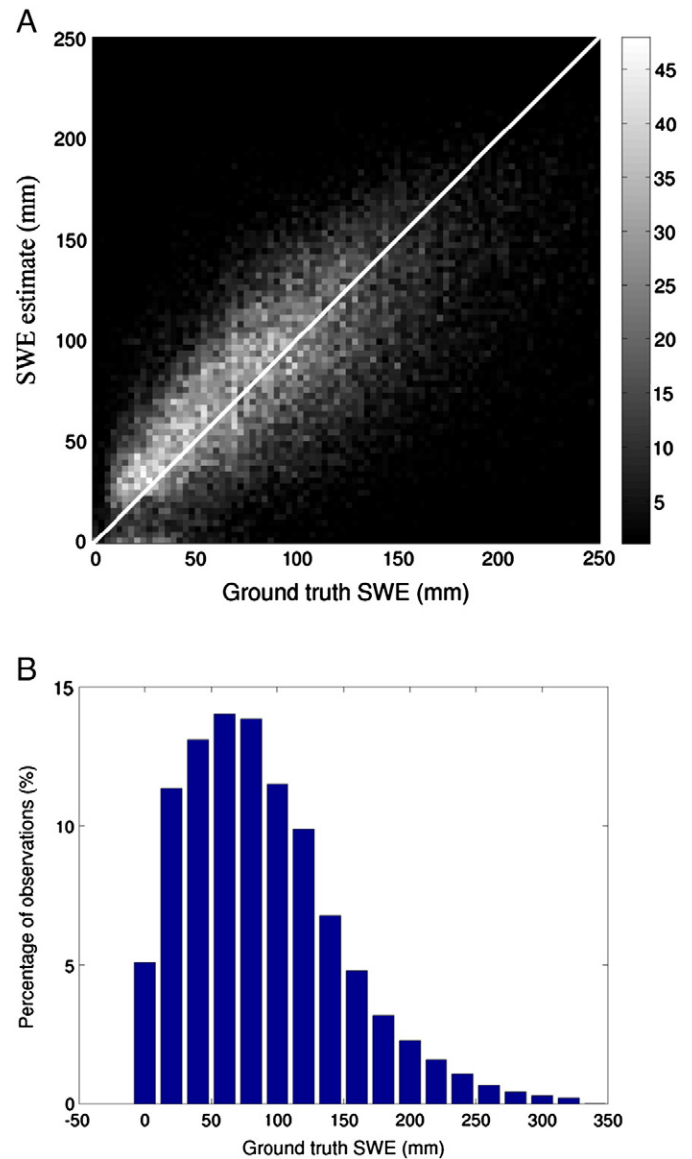

Fig. 7. SWE algorithm performance over Russia and former Soviet Union when compared with independent INTAS-SCCONE snow course observations from the period of 1979–2000 for March only. (a) Scatterplot of estimates. The number of estimates obtained for intervals of 3 mm is coded by the intensity of white color. RMSE = 54.6 mm and bias = −11.1 mm. Number of samples is 37 504 (b) Observed distribution of ground truth SWE from snow courses.

0.28 respectively. Evaluation statistics were also calculated for each land cover category given the unique characteristics of the reference measurements available for each region. These results are summarized in Table 3, and show that retrieval uncertainty is high for deep boreal forest snow, consistent with the evaluation for Finland and Eurasia. This is the only Canadian region under investigation for which SWE regularly exceeds the 150 mm threshold. When the statistics were re-computed using a 150 mm threshold, algorithm performance improved appreciably with the RMSE value decreasing to 21 mm.

In the southern boreal forest, the retrieval challenge is not deep snow, but the presence of relatively dense forest vegetation. Time series plots for four BERMS sites located within a single EASE-Grid are shown in Fig. 9. The average daily snow depth (from hourly automated snow depth measurements) was converted to SWE using the mean measured density from bi-weekly snow surveys conducted at each site. The BERMS measurements illustrate the range in SWE that is typical within the coarse footprint SWE retrieval due to snow interactions with mixed
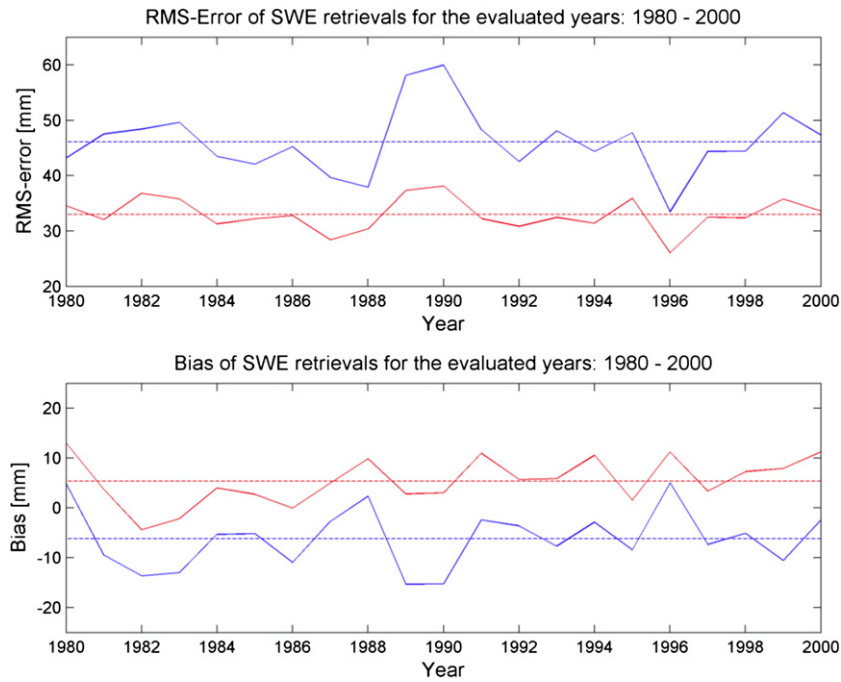
Fig. 8. RMS error and bias of SWE estimates for Eurasia from the comparison against independent INTAS-SCCONE snow course observations, 1979–2000: (a) results for the complete data set and (b) results for cases with reference SWE lower than 150 mm (88.5% of all cases). RMSE and bias for the whole data set is shown by red lines. Bias is the (mean) difference estimated value minus the reference value.

forest vegetation. In spite of this heterogeneity, the SWE estimates agreed well with the BERMS measurements through each season. There is a tendency for early season shallow snow to be missed by the assimilation scheme, and the retrievals to drop too rapidly in the spring. The relative availability of climate station observations in the southern boreal forest (compared to the northern boreal forest) and the typically shallow snow cover (SWE<100 mm) helps to reduce uncertainty in this region.

The relatively high uncertainty over tundra regions (Table 3) is likely driven by three issues: the extremely sparse network of surface climate stations across the Canadian sub-Arctic, the complex microwave emission from lake rich snow covered tundra (see Derksen et al., 2009), and the extremely heterogeneous tundra snow cover which complicates the determination of 'ground-truth' SWE at coarse spatial resolutions. In open tundra regions, topographic controls on the wind redistribution of snow can be significant. Intensive ground measurement campaigns in a tundra environment near Daring Lake, NT have allowed investigation of relationships between coarse resolution satellite SWE retrievals and sub-grid statistical distributions of ground measured SWE (Rees et al., 2006). Fig. 10 shows histograms of ground measured sub-grid SWE relative to the single retrieval available for this 25 km grid cell. The assimilation approach reasonably captures a SWE value near the center of the distribution, but the spread in ground measured SWE (for which no information can be estimated using satellite data) is clearly evident.

Table 2
Seasonal summary of SWE assimilation algorithm performance over Eurasia, 1980–2000 (fall: September–December; winter: September–March; spring: April–May). In parenthesis are the values for cases with reference SWE<150 mm. R is significant at 99% level in all cases.

Season	RMSE (mm)	bias(mm)	Corr. coeff	Samples
Fall	23.0 (21.7)	5.8 (6.5)	0.69 (0.70)	35 197 (34 943)
Winter	37.7 (28.9)	1.7 (7.7)	0.72 (0.72)	165 784 (150 405)
Spring	72.5 (47.3)	−37.6 (−19.3)	0.53 (0.47)	42 843 (33 189)

4.3. Algorithm inter-comparison

The performance of the SWE assimilation technique was also compared with the accuracy characteristics of a typical stand-alone passive microwave algorithm. This was carried out in order to demonstrate the magnitude of improvement that can be obtained by using the assimilation approach. The reference data set used here was the NSIDC global monthly SWE climatology (Armstrong et al., 2007). The algorithm is based on a channel difference of 18 or 19 GHz and 37 GHz horizontally polarized measurements following Chang et al. (1987) and Armstrong and Brodzik (2001). The algorithm includes a correction for surface forest cover (Chang et al. 1996). SWE values lower than 7.5 mm are set to zero and additional processing steps to compensate for glacier and desert effects have been performed (see Armstrong et al., 2007 for details). Fig. 11 shows the obtained performance characteristics for the NSIDC data for the region of Eurasia Russia when assessed using the INTAS-SCCONE snow path measurement data set described in Section 2. The INTAS-SCCONE data were averaged on a monthly basis for comparison. The assimilation algorithm (see Fig. 7 a) provides a clear improvement in the accuracy characteristics (RMSE and bias error) when compared with those obtained by a typical stand-alone algorithm utilizing a spectral T_B difference for SWE retrieval.

4.4. Snow cover trends from SWE time-series

Fig. 12 shows an example of mean snow mass seasonal evolution for 1982–2010. The snow mass is calculated by summing the SWE values for all snow covered grid cells, and by multiplying these values with the grid cell area. According to Fig. 12, the hemispherical snow mass has its maximum value during February–March. Fig. 13 shows the monthly snow mass estimates for March covering the time period from 1982 to 2009 as determined from maps of monthly averaged SWE. The trend line fitted to snow mass estimates suggests a decrease of 7% for a period of 30 years for the region of permanent seasonal snow cover (excluding mountain regions with high topographic
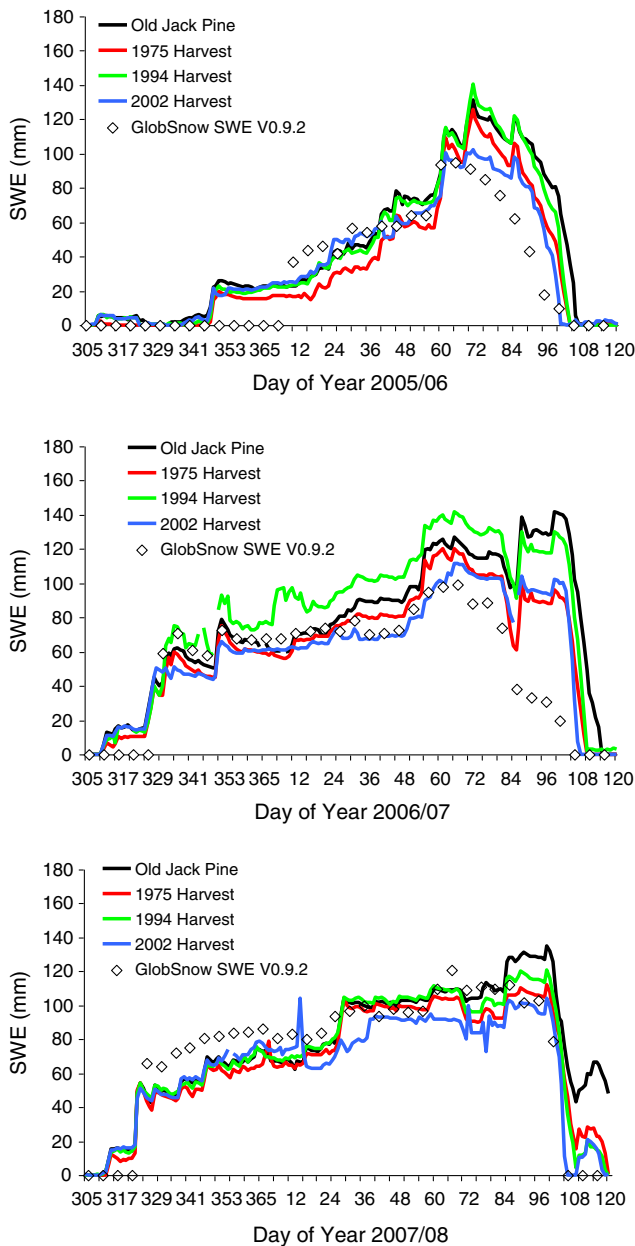
Table 3
Summary of SWE assimilation algorithm performance over Canada, 2005/06–2007/08.

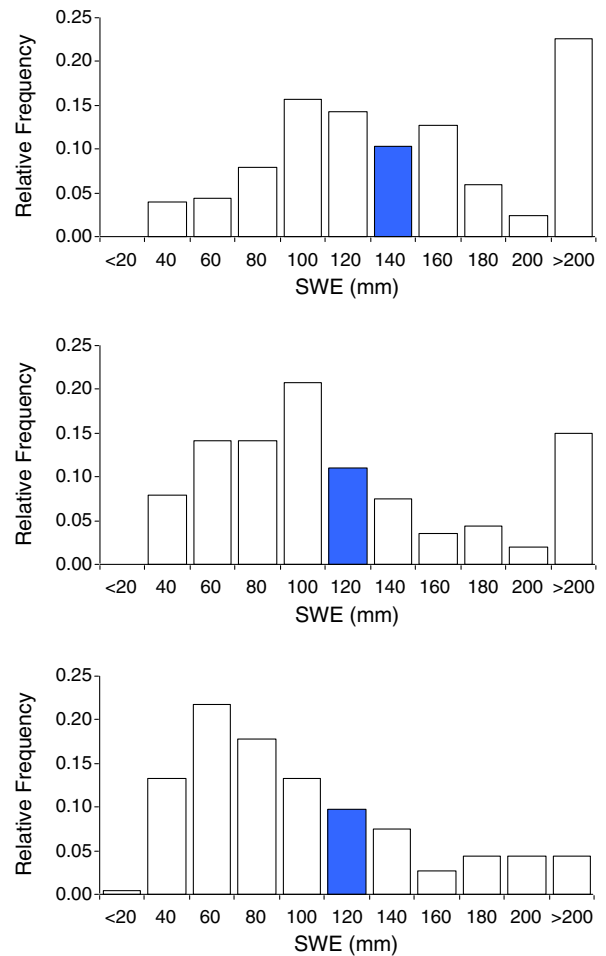| Land cover	Reference dataset	Year	n	Mean SWE (mm)	RMSE (mm)	R	R significant at 95% level	R significant at 99% level	Mean bias
Tundra	Intensive sites; SnowSTAR 2007	2005–2007	28	120	47	0.05	No	No	−36
Northern Boreal	EC Snow Surveys	2006–2007 SWE	105	134	70	0.00	No	No	−32
		<150 mm	73	101	21	0.52	Yes	Yes	3
Southern Boreal	EC Snow Surveys	2005–2007	57	75	28	0.43	Yes	Yes	−8
Southern Boreal	BERMS	All	468	70	25	0.87	Yes	Yes	−3
Prairie	EC Snow Surveys	All	41	47	21	0.51	Yes	Yes	6

variations within a grid cell). Note that this trend is opposite to the possible small bias that may be associated with the SWE retrievals, as illustrated in Fig. 8.

Fig. 9. Time series of BERMS measurements compared to SWE retrievals, 2005/06 (top) through 2007/08 (bottom).

5. Discussion

An essential issue concerning the combined use of satellite and in situ data, is the magnitude of the impact of satellite observations to generated hemispheric maps of SWE. Fig. 5 indicates that a reasonable baseline level of SWE is obtained from the interpolation of ground-based snow depth measurements alone. However, satellite observations can change these values significantly with the impact of these measurements varying both spatially and temporally. A key characteristic of the algorithm is that it optimizes the weight of different data sources through a dynamic calculation of pixel-wise satellite data modeling error variances. This is combined with the dynamic calculation of model derivatives that define the sensitivity of satellite data to SWE and snow grain size (as well for each pixel), see Eq. (4.a)

Fig. 10. Sub-grid SWE distributions from intensive tundra field campaigns near Daring Lake, NT, 2006 (top) through 2008 (bottom). Shaded columns indicate the single SWE estimate produced for this grid cell.
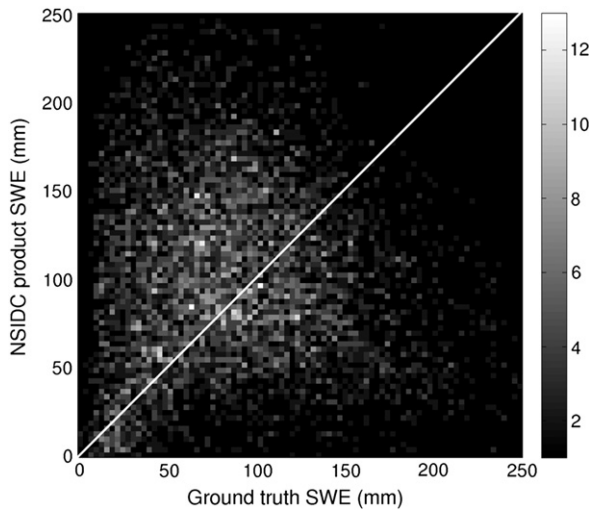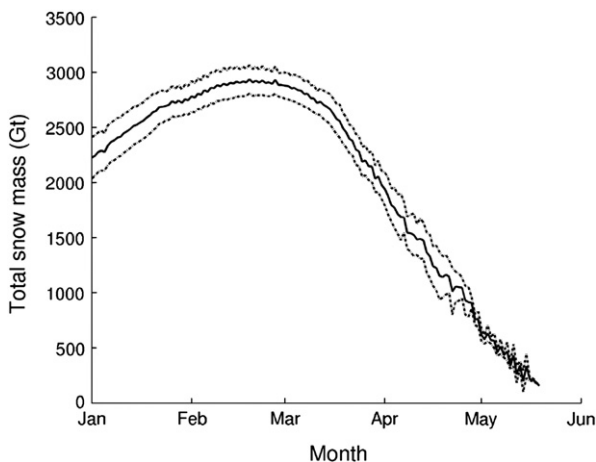
Fig. 11. NSIDC global monthly SWE climatology performance over Russia and former Soviet Union when compared with independent INTAS-SCCONE snow course observations from the period of 1979–2000 for March only. The number of estimates obtained for intervals of 3 mm is coded by the intensity of white color. RMSE = 92.5 mm and bias = 12.0 mm. Number of samples is 11 730. The reference data is averaged over the March of each year (same data without monthly averaging is also used in Fig. 7).

Fig. 13. Trend of snow mass evolution in 1982–2009 (northern hemisphere) as determined from the mean SWE values for March.
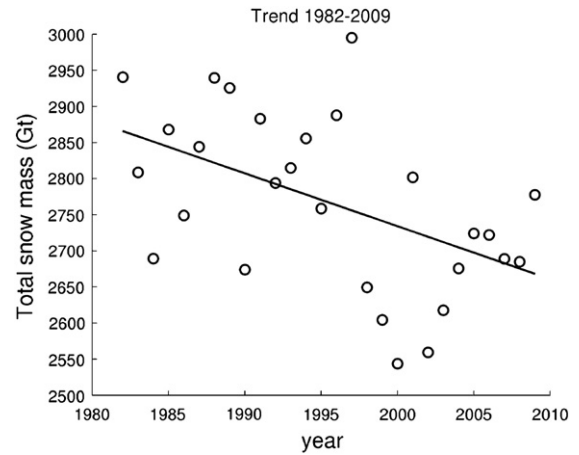
and Eq. (4.b). Hence the derived SWE maps give a maximum likelihood estimate of SWE for every grid cell. Additionally, the statistical error level of SWE estimate is calculated separately for every pixel. Another important novelty of this new methodology is the combined mapping of the snow area and snow melt based on satellite radiometer data.

Snow grain size is a very important parameter within the forward T_B simulation component of the retrieval, as the sensitivity of T_B to snow grain size is high. The problem of varying grain size is tackled by the assimilation algorithm through the estimation of effective snow grain size at the locations of weather stations. Grain size and variance estimates for a station under investigation are obtained by averaging estimates from near-by stations. This is needed to reduce noise in the estimation of the spatial behavior of snow grain size. The reference field of grain size is obtained through kriging interpolation of grain size estimated for different weather stations, and represents another useful level of information produced from the retrieval scheme.

The grain size estimated by the algorithm is actually an effective value that incorporates the effect of modeling errors and inaccuracies in the algorithm input data. In the second step of the algorithm, the background field of snow grain size is estimated by fitting the

modeled brightness temperature gradient into observations. Thus, the outcome of this fitting procedure, the effective grain size, includes the effects of inaccuracies in forest stem volume information and snow density (treated as a constant parameter in the algorithm with a value of 0.24 g/cm^3). Nevertheless, the final outcome (step 4 of the algorithm) includes the estimated effective snow grain size value, in addition to the estimated SWE. The effective grain sizes are realistic despite the limitations of the scene brightness temperature model and the uncertainties in the input data. For example, in the case of observations from March (all years and all snow areas) the algorithm showed a mean (effective) grain size of 1.24 mm with a standard deviation of 0.34 mm.

The density of snow was treated as a constant parameter in this study in order to avoid parameters that are spatially or temporally varying (only land cover characteristics were spatially varying). Thus, only the actual algorithm input data from satellite observations and synoptic weather stations was changing, (brightness temperatures and snow depth observations). In future development of the algorithm snow density can be treated with spatially and temporally changing a priori values. As well, the statistical error assigned to the point-wise synoptic weather station observations on snow depth can vary at least spatially (the available Canadian observations indicate that this error can be higher for tundra regions than for boreal forests). In this study this statistical error was set to 150 cm^2 for all regions based on analyses of distributed Finnish and Canadian coincident snow surveys as reference. However, the distributed snow survey information has its inherent (largely unknown) error characteristics, which sets limitations to all performance considerations.

Figs. 7a and 11 present a comparison of the performance of the assimilation approach with the accuracy characteristics of a typical stand-alone passive microwave algorithm, and indicate a significant improvement produced by the assimilation algorithm. Similar results were obtained for northern Eurasia when the proposed technique was compared with other stand-alone SWE mapping products and methods, such as the Environment Canada land cover sensitive set of algorithms (Derksen et al., 2005). This algorithm suite, designed for Canada, was tested here for the Eurasia, even though it is designed only for use in Canada (the algorithms were empirically derived from regional Canadian datasets). In the case of Canada, the Environment Canada algorithms provided slightly better results for some regions than the assimilation algorithm, which is expected when comparing regional algorithms with a global approach. A more detailed comparison with alternative techniques including reanalysis products (i.e. Simmons et al., 2007) is an issue for further investigation.

Across northern Eurasia, the independent distributed SWE reference data enabled performance analysis of the assimilation algorithm

Fig. 12. Mean snow mass evolution, 1982–2010, for the northern hemisphere (excluding mountain regions). Dashed lines correspond to the standard deviation.

over 20 seasons (Fig. 8). Only March was selected for this analysis since the snowpack is thickest this month (as suggested by Fig. 12). Yearly RMSE and bias for was relatively small with little interannual variability. The low level of annual systematic error suggests that the trends and total hemispherical snow masses given in Figs. 12 and 13 are realistic and reliable. The uncertainty of the trend can be evaluated by comparing Fig. 13 with Fig. 8. The estimated hemispheric total snow mass trend shown in Fig. 13 is − 7.3 Gtons/year.

Grid cells with a high variation of elevation were masked out because of a priori known poor algorithm performance in complex terrain. The primary sources of this uncertainty are the coarse resolution of the satellite T_B data, and the inability of discrete climate station observations to capture the strong elevational gradients in SWE within 25 km resolution grid cells. The authors have tested the algorithm sensitivity to stem volume by reprocessing SWE estimates for year 2004 where stem volume was assigned value of 100 m^3/ha. The results of this test were evaluated on those pixels whose forest cover fraction is larger than 80% in Canada. The maximum difference was less than 0.12% which indicates a low sensitivity to stem volume. For non-mountainous areas, the overall performance was strong, although retrieval sensitivity to land cover and forest properties remain an issue for further investigation (see also Pardé et al., 2007; Roy et al., 2004; Vachon et al., 2010). Additionally, the consideration or compensation for the effect of (frozen) lakes requires further study and algorithm development work.

6. Summary

In this study an algorithm assimilating space-borne passive microwave radiometer data with synoptic weather station observations of snow depth to estimate SWE was assessed and applied at the hemispheric scale. As an outcome, a Climate Data Record (CDR) extending through a time span of 30 years was produced and evaluated (1980–2010). The validation was carried out using independent reference data from primarily the Russian portion of northern Eurasia, Finland and Canada. The reference data includes an extensive set of snow course observations of SWE. Thus, a comprehensive view on algorithm performance was obtained. The employed assimilation approach shows an improved accuracy level when compared with uncertainty statistics calculated for a typical stand-alone brightness temperature channel difference algorithm. The algorithm applied here provides good overall performance for the hemispheric scale estimation of SWE (including a per-grid cell uncertainty estimate) and is well suited for climatological analysis and climate model evaluation.

References

Armstrong, R., & Brodzik, M. (2001). Recent northern hemisphere snow extent: A comparison of data derived from visible and microwave satellite sensors. *Geophysical Research Letters*, 28(19), 3673–3676.
Armstrong, R., & Brodzik, M. (2002). Hemispheric-scale comparison and evaluation of passive-microwave snow algorithms. *Annals of Glaciology*, 34, 38–44.
Armstrong, R. L., Brodzik, M. J., Knowles, K., & Savoie, M. (2007). *Global monthly EASE-Grid snow water equivalent climatology.* Boulder, CO: National Snow and Ice Data Center Digital media.
Armstrong, R. L., Knowles, K. W., Brodzik, M. J., & Hardman, M. A. (1994). updated 2009. DMSP SSM/I Pathfinder daily EASE-Grid brightness temperatures, Jan 1987–Jul 2008. Boulder, Colorado USA: National Snow and Ice Data Center Digital media.
Barnett, T., Adam, J., & Lettenmaier, D. (2005). Potential impacts of a warming climate on water availability in snow-dominated regions. *Nature*, 438, 303–309, doi: 10.1038/nature04141.
Bartalev, S., Ershov, D., Isaev, A., Potapov, P., Turubanova, S., & Yaroshenko, A. (2004). Russia's Forests. TerraNorte Information System. RAS Space Research Institute http://terranorte.iki.rssi.ru
Brasnett, B. (1999). A global analysis of snow depth for numerical weather prediction. *Journal of Applied Meteorology*, 38, 726–740.
Brown, R., Derksen, C., & Wang, L. (2010). A multi-dataset analysis of variability and change in Arctic spring snow cover extent, 1967–2008. *Journal of Geophysical Research*, doi:10.1029/2010JD013975.
Brown, R., & Tapsoba, D. (2007). Improved mapping of snow water equivalent over Quebec. *64th EASTERN SNOW CONFERENCE St. John's, Newfoundland, Canada.*
Carroll, T., Cline, D., Olheiser, C., Rost, A., Nilsonn, A., Fall, G., Bovitz, C., & Li, L. (2006). NOAA's national snow analysis. *Proceedings, 74th Western Snow Conference.*
Chang, A., Foster, J., & Hall, D. (1987). Nimbus-7 SMMR derived global snow cover parameters. *Annals of Glaciology*, 9, 39–44.
Chang, A., Foster, J., & Hall, D. (1990). Satellite sensor estimates of northern hemisphere snow volume. *International Journal of Remote Sensing*, 11(1), 167–171.
Chang, A. T. C., Foster, J. L., & Hall, D. K. (1996). Effects of forest on the snow parameters derived from microwave measurements during the BOREAS Winter Field Campaign. *Hydrological Processes*, 10, 1565–1574.
De Sève, D., Bernier, M., Fortin, J. P., & Walker, A. (1997). Preliminary analysis of snow microwave radiometry using the SSM/I Passive Microwave Data: The case of La Grande River Watershed (Québec). *Annals of Glaciology*, 25, 353–361.
De Sève, D., Évora, N., & Tapsoba, D. (2007). Comparison of three algorithms for estimating Snow Water Equivalent (SWE) over the La Grande River watershed using SSM/I data in the context of Hydro-Québec's hydraulic power management. *IGARSS'07, Barcelona, Spain, July 23–July 27, 2007.*
Derksen, C. (2008). The contribution of AMSR-E 18.7 and 10.7 GHz measurements to improved boreal forest snow water equivalent retrievals. *Remote Sensing of Environment*, 112, 2700–2709.
Derksen, C., Sturm, M., Liston, G., Holmgren, J., Huntington, H., Silis, A., & Solie, D. (2009). Northwest Territories and Nunavut snow characteristics from a sub-Arctic traverse: Implications for passive microwave remote sensing. *Journal of Hydrometeorology*, 10(2), 448–463.
Derksen, C., Toose, P., Rees, A., Wang, L., English, M., Walker, A., & Sturm, M. (2010). Development of a tundra-specific snow water equivalent retrieval algorithm for satellite passive microwave data. *Remote Sensing of Environment*, 114, 1699–1709.
Derksen, C., Walker, A., & Goodison, B. (2005). Evaluation of passive microwave snow water equivalent retrievals across the boreal forest/tundra transition of western Canada. *Remote Sensing of Environment*, 96(3/4), 315–327.
Durand, M., & Margulis, S. (2006). Feasibility test of multifrequency radiometric data assimilation to estimate snow water equivalent. *Journal of Hydrometeorology*, 7, 443–457.
Dyer, J., & Mote, T. (2006). Spatial variability and trends in observed snow depth over North America. *Geophysical Research Letters*, 33, doi:10.1029/2006GL027258.
Erxleben, J., Elder, K., & Davis, R. E. (2002). Comparison of spatial interpolation methods for estimating snow distribution in the Colorado Rocky Mountains. *Hydrological Processes*, 16, 3627–3649.
Foster, J., Chang, A., & Hall, D. (1997). Comparison of snow mass estimates from a prototype passive microwave snow algorithm, a revised algorithm and a snow depth climatology. *Remote Sensing of Environment*, 62, 132–142.
Foster, J., Chang, A., Hall, D., & Rango, A. (1991). Derivation of snow water equivalent in boreal forests using microwave radiometry. *Arctic*, 44, 147–152.
Goodison, B. (1989). Determination of areal snow water equivalent on the Canadian Prairies using passive microwave satellite data. *Proceedings, IGARSS'89, Vancouver.* 3:1243–1246.
Goodison, B., & Walker, A. (1995). Canadian development and use of snow cover information from passive microwave satellite data. In B. Choudhury, Y. Kerr, E. Njoku, & P. Pampaloni (Eds.), *Passive Microwave Remote Sensing of Land–Atmosphere Interactions. VSP BV, Utrecht, Netherlands* (pp. 245–262).
Grogan, P., & Jonasson, S. (2006). Ecosystem CO$_2$ production during winter in a Swedish subarctic region: The relative importance of climate and vegetation type. *Global Change Biology*, 12, 1479–1495.
Hall, D., Kelly, R. E. J., Riggs, G. A., Chang, A. T. C., & Foster, J. L. (2002). Assessment of the relative accuracy of hemispheric-scale snow-cover maps. *Annals of Glaciology*, 34, 24–30.
Hallikainen, M., & Jolma, P. (1992). Comparison of algorithms for retrieval of snow water equivalent from Nimbus-7 SMMR data in Finland. *IEEE Transactions on Geoscience and Remote Sensing*, 30(1).
Hudson, G., & Wackernagel, H. (1994). Mapping temperature using kriging with external drift: theory and an example from Scotland. *International Journal of Climatology*, 14, 77–91.
Kelly, R., Chang, A., Tsang, L., & Foster, J. (2003). A prototype AMSR-E global snow area and snow depth algorithm. *IEEE Transactions on Geoscience and Remote Sensing*, 41(2), 230–242.
Kitaev, L., Kislov, A., Krenke, A., Razuvaev, V., Martuganov, R., & Konstantinov, I. (2002). The snow characteristics of northern Eurasia and their relationship to climatic parameters. *Boreal Environment Research*, 7, 437–445.
Knowles, K., Njoku, E., Armstrong, R., & Brodzik, M. J. (2002). *Nimbus-7 SMMR Pathfinder daily EASE-Grid brightness temperatures.* Boulder, CO: National Snow and Ice Data Center Digital media and CD-ROM.
Knowles, K. W., Savoie, M. H., Armstrong, R. L., & Brodzik, M. J. (2006). updated 2009. *AMSR-E/Aqua daily EASE-Grid brightness temperatures*, 2002–2008. Boulder, Colorado USA: National Snow and Ice Data Center Digital media.
Koenig, L., & Forster, R. (2004). Evaluation of passive microwave snow water equivalent algorithms in the depth hoar-dominated snowpack of the Kuparuk River watershed, Alaska, USA. *Remote Sensing of Environment*, 93, 511–527.

Kuusisto, E. (1984). *Snow accumulation and snowmelt in Finland, vol. 55,* Helsinki: Water Research Institute.

Lemmetyinen, J., Pulliainen, J., Rees, A., Kontu, A., Qiu, Y., & Derksen, C. (2010). Multiple layer adaptation of HUT Snow Emission Model: Comparison with experimental data. *IEEE Transactions on Geoscience and Remote Sensing, 48,* 2781–2794.

Luojus, K., Pulliainen, J., Takala, M., Derksen, C., Rott, H., Nagler, T., Solberg, R., Wiesmann, A., Metsämäki, S., Malnes, E., & Bojkov, B. (2010). Investigating the feasibility of the GlobSnow snow water equivalent data for climate research purposes. *Geoscience and Remote Sensing Symposium (IGARSS), 2010 IEEE International* (pp. 4851–4853). 25–30 July 2010. doi:10.1109/IGARSS.2010.5741987.

Mätzler, C. (1994). Passive microwave signatures of landscapes in winter. *Meteorology and Atmospheric Physics, 54,* 241–260.

Mognard, N., & Josberger, E. (2002). Seasonal evolution of snowpack parameters, northern Great Plains. *Annals of Glaciology, 34,* 15–23.

Nagler, T., and H. Rott, 1992: Development and intercomparisons of snow mapping algorithms based on SSM/I data. Proc. IGARSS 1992, Houston, TX, IEEE, Catalog 92CH 3041–1, 812–814.

National Geophysical Data Center, 1988. Data Announcement 88-MGG-02, Digital relief of the Surface of the Earth (http://www.ngdc.noaa.gov/mgg/global/etopo5.HTML).

Pardé, M., Goïta, K., & Royer, A. (2007). *Inversion of a passive microwave snow emission model for water equivalent estimation using airborne and satellite data. Remote Sensing of Cryosphere Special Issue of Remote Sensing of Environment, vol. 111.* (pp. 346–356).

Perala, J., & Reuna, M. (1990). The areal and time variability of snow water equivalent in Finland. *National Board of Waters and Environment, Water, and Environment Research Inst., Hydrological Office, ser. A 56, Helsinki* (pp. 260). in Finnish.

Pulliainen, J. (2006). Mapping of snow water equivalent and snow depth in boreal and sub-arctic zones by assimilating space-borne microwave radiometer data and ground-based observations. *Remote Sensing of Environment, 101,* 257–269.

Pulliainen, J., Grandell, J., & Hallikainen, M. (1999). HUT Snow Emission Model and its applicability to snow water equivalent retrieval. *IEEE Transactions on Geoscience and Remote Sensing, 37*(3).

Pulliainen, J., & Hallikainen, M. (2001). Retrieval of regional snow water equivalent from spaceborne passive microwave observations. *Remote Sensing of Environment, 75*(1), 76–85.

Rees, A., Derksen, C., English, M., Walker, A., & Duguay, C. (2006). Uncertainty in snow mass retrievals from satellite passive microwave data in lake-rich high-latitude environments. *Hydrological Processes, 20,* 1019–1022.

Rosenfeld, S., & Grody, N. (2000). Anomalous microwave spectra of snow cover observed from Special Sensor Microwave/Imager measurements. *Journal of Geophysical Research, 105*(D11), doi:10.1029/1999JD900486 issn:0148–0227.

Rott, H., Nagler, T., & Aschbacher, J. (1991). Algorithm development for monitoring the global snow cover by spaceborne microwave radiometry. *Proceedings, 11th EARSel Symposium, Graz, Austria, July, 1991* (pp. 58–69).

Roy, V., Goita, K., Royer, A., Walker, A., & Goodison, B. (2004). Snow water equivalent retrieval in a Canadian boreal environment from microwave measurements using the HUT snow emission model. *IEEE Transactions on Geoscience and Remote Sensing, 42*(9), 1850–1859.

Rutter, N., Cline, D., & Li, L. (2008). Evaluation of the NOHRSC snow model (NSM) in a one-dimensional mode. *Journal of Hydrometeorology, 9,* 695–711.

Simmons, A., S. Uppala, D. Dee, and S. Kobayashi. 2007: ERA-Interim: New ECMWF reanalysis products from 1989 onwards. ECMWF Newsletter No. 110 – Winter 2006/07, 25–35.

Sturm, M., Taras, B., Liston, G., Derksen, C., Jonas, T., & Lea, J. (2010). Estimating snow water equivalent using snow depth data and climate classes. *Journal of Hydrometeorology, 11,* 1380–1394.

Tait, A. (1998). Estimation of snow water equivalent using passive microwave radiation data. *Remote Sensing of Environment, 64,* 286–291.

Takala, O. M., Pulliainen, J., Metsämäki, S., & Koskinen, J. (2009). Detection of snowmelt using spaceborne microwave radiometer data in Eurasia From 1979 to 2007. *IEEE Transactions on Geoscience and Remote Sensing, 47,* 2996–3007.

Tong, J., Dery, S., Jackson, P., & Derksen, C. (2010). Testing snow water equivalent retrieval algorithms for passive microwave remote sensing in an alpine watershed of western Canada. *Canadian Journal of Remote Sensing, 36*(S1), 74–86.

Vachon, F., Goïta, K., De Sève, D., & Royer, A. (2010). Inversion of a Snow Emission Model calibrated with in situ data for snow water equivalent monitoring. *IEEE Transactions on Geoscience and Remote Sensing, 48*(1), 59–71.

Wiesmann, A., & Matzler, C. (1999). Microwave emission model of layered snowpacks. *Remote Sensing of Environment, 70,* 307–316.